RSC Advances

COMMUNICATION

View Article Online
View Journal | View Issue

Cite this: *RSC Adv.*, 2016, **6**, 48427

Antenna-type radiofrequency generator in nanoparticle-mediated hyperthermia†

B. Nasseri,[a] M. Yilmaz,[b] M. Turk,[c] I. C. Kocum[d] and E. Piskin*[a]

Received 3rd February 2016
Accepted 30th April 2016

DOI: 10.1039/c6ra03197h

www.rsc.org/advances

Induction of hyperthermia using nanoparticles with specific magnetic, electrical, acoustic, optical or thermal properties is a potential alternative to conventional thermal ablation in cancer therapy. In this study, for the first time we employed an antenna-type radiofrequency (RF) generator as the energy source and as a proof of concept the effects of nanoparticles of varying structures and sizes, such as superparamagnetic iron oxide nanoparticles (SPIONs), gold-coated superparamagnetic iron oxide nanoparticles (Au@SPIONs), spherical gold nanoparticles (AuNPs), and gold nanorods (AuNRs) on RF hyperthermia were examined to determine hyperthermia efficiency of the antenna-type RF generator. In preliminary experiments, RF was applied at varying powers to various nanoparticle solutions. In all cases, temperature rises due to exposure of RF radiation to nanoparticles were captured by using an infrared thermal camera. This procedure was applied to *in vitro* tests of fibroblast (L-929) and breast cancer (MCF-7) cell lines. Cell viability, apoptosis and necrosis were evaluated in both cell lines to comprehensively determine cell toxicity. Due to their particle size and chemical nature, SPIONs, in the case of highest RF power and nanoparticle concentration, resulted in the lowest cell viability and highest levels of apoptosis and necrosis.

Introduction

Surgery, chemotherapy and radiotherapy are gold standard methods in cancer therapy.[1] However, their short-term and long-term side effects are highly controversial, limiting their clinical application.[2] Remarkable progress in biotechnology and nanotechnology has led to the advent of treatment procedures such as gene therapy, immunotherapy and hormone therapy.[1] However, despite several studies, these new techniques remain immature and lack clinical application. Alternatively, the recent employment of energy modalities including electromagnetic waves, diathermic, electrical, sound energy as well as mechanical energy, for thermal ablation of cancer cells *via* hyperthermia has become a potential cancer therapy technique.[3,4] This non-invasive method exploits the higher sensitivity of cancer cells to above-normal physiological temperatures (>41 °C).[5,6] Hyperthermia treatments are alternative and complementary methods in cancer therapy and also less risky than standard cancer treatments and cause fewer side effects, allowing repeated application.[2,7,8]

Nanotechnology is a rapidly evolving scientific field and has had a tremendous impact on the diagnosis and treatment of cancer in particular.[2,9–11] Moreover, nanoparticle-mediated hyperthermia has attracted enormous attention as a promising biomedical application for the treatment of cancer.[3,11–14] In nanoparticle-mediated hyperthermia, the interaction of metallic nanoparticles including magnetite and gold nanoparticles, with electromagnetic waves, such as NIR laser and visible light laser and radiofrequency (RF), leads to absorption of wave energy and heat generation according to different mechanisms such as Surface Plasmon Resonance (SPR)[15] and Specific Absorption Rate (SAR).[16] Various types of nanoparticles, including superparamagnetic iron oxide nanoparticles (SPIONs), spherical gold nanoparticles (AuNPs), gold nanorods (AuNRs) and core–shell structures have been employed in cancer treatment studies.[2,9–11,17] Use of such nanoparticles for hyperthermia applications requires precise control of their physiochemical properties, because the induced heat is highly dependent on these properties.[5,18] Employment of electromagnetic waves in the RF domain, as a non-ionized, non-destructive, and non-harmful energy band of electromagnetic spectrum, in nanoparticle-mediated hyperthermia is advantageous compared with other hyperthermia techniques. The advantages include lower harmful effects because of low frequencies and high wavelengths of RF waves, its non-destructive effects on excited tissues, and appropriate

[a]*Chemical Engineering Department and Bioengineering Division, Centre for Bioengineering and Biyomedtek, Hacettepe University, Beytepe, 06800, Ankara, Turkey. E-mail: piskin@hacettepe.edu.tr; Fax: +90 312 2992124; Tel: +90 312 2977400*

[b]*Bioengineering Department, Sinop University, Sinop, Turkey*

[c]*Bioengineering Department, Kirikkale University, Kirikkale, Turkey*

[d]*Biomedical Engineering Department, Baskent University, Ankara, Turkey*

† Electronic supplementary information (ESI) available. See DOI: 10.1039/c6ra03197h

penetration depths into the body for the deep hyperthermia of the seated tumors such as liver, lung, abdomen, pelvis and brain, low cost and easy fabrication of RF generators and efficacious properties of nanoparticles.[19–23] To use these impressive advantages of nanoparticle-mediated hyperthermia numerous studies have been performed with different nanoparticles in different characteristics and morphologies. For instance, Cardinal *et al.* employed gold nanoparticles to determine their hyperthermia efficiency in *in vivo* study of HepG2 liver cancer cells by using 13.56 MHz capacitive RF generator.[21] The RF use at 35 W combined with nanoparticles resulted in adequate temperature increase for thermal ablation of cancer cells. Similarly, Gannon *et al.* investigated the radiofrequency thermal destruction of human gastrointestinal cancer cells in the case of gold nanoparticles at different capacitive RF powers.[20] It was detected that nanoparticle-mediated RF hyperthermia led to >96% of the cell death without cytotoxicities of nanoparticles. Mustafa *et al.* employed a bobbin type generator in magnetic nanoparticle-mediated hyperthermia.[24] They reported that both nanoparticle size and RF frequency are critical parameters that influence the hyperthermia efficiency. In spite of these studies, the nanoparticle-mediated RF hyperthermia is still immature and needs further developments to be applied in clinical usage.

Typically inductive modulus (annular cylindrical bobbin type) and capacitive coupled are main RF generator types which have been well known in clinically uses. RF generators enable to produce RF waves with desired frequencies (*i.e.* wavelength) and intended RF powers related to application area by using appropriate technologies. In inductive RF generators RF properties depend on coil turns, coil material, "outer diameter" (OD), coil round diameter as well as output power of RF generator. Various coils can resonate in different frequencies which relates to RF device technical specifications. The properties of RF waves that produced by capacitive type RF generators depend on transmission head and receiving head distance, type and power of end-firing transmission head, cover material of receiving head as well as RF supplier's power. Both inductive modulus and capacitive coupled RF generators are sophisticated, too technologically demanding and quite expensive to construct. Innovative strategies to develop reliable, easy-to-construct and low-cost RF generators are the hot-topic of the hyperthermia based studies. To overcome this bottleneck of available RF generators, in this study, for the first time, we developed a simple yet facile antenna-type RF generator. The antenna-type RF generator with a 200 W output and 144.015 MHz RF frequency was employed as the electromagnetic source during the hyperthermia studies (see Scheme 1). The proposed home-made RF generator is user friendly, reliable, simple, and low-cost and has intense potential to be used in clinical applications. A detailed set of study for the proof of concept was performed to determine the hyperthermia efficiencies of SPIONs, gold-coated SPIONs (Au@SPIONs), AuNPs, and AuNRs. Specifically, the effects of nanoparticles of varying structures

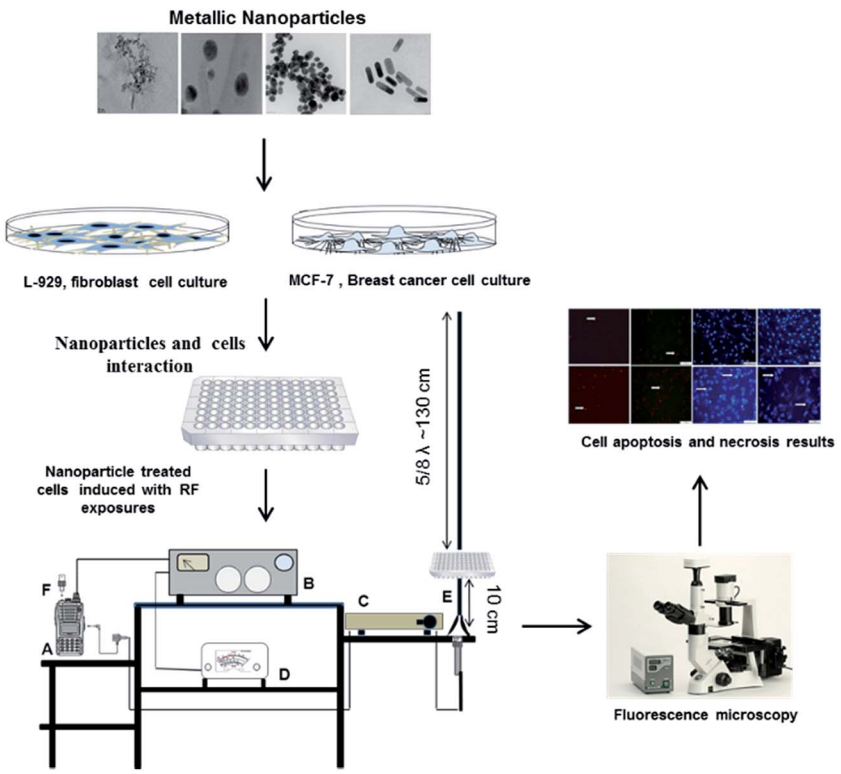

Scheme 1 Procedures of the hyperthermia and details of the antenna-type RF generator (A) KG-UVD1P model hand-held transceiver, (B) micro base and repeater stations 132–174 MHz 68P81036E40-B, (C) RF amplifier (0–200 W), (D) Voltage Standing Wave Ratio (VSWR), (E) TA2FC antenna, (F) power supplier connection.

and concentrations after RF exposures were investigated in terms of temperature rises in cell-free solutions using an infrared thermal camera. Subsequent *in vitro* experiments were performed to assess cell viability, apoptosis, and necrosis in fibroblast (L-929) and breast cancer (MCF-7) cell lines.

Experimental section

Materials and synthesis of nanoparticles

The details of this section were given in ESI† section.

Design of RF generator

The construction of a simple yet facile an antenna-type RF generator was main topic of the present study. The antenna-type RF generator with a 200 W output was employed as the electromagnetic source during the hyperthermia studies. For this, 144.015 MHz RF frequency was chosen, since a single radiating element of $5/8\lambda$ correspond to an antenna with length of approximately 130 cm and the related frequency can be applied to numerous procedures. Distribution of parasitic signals was prevented to facilitate communication. The RF generator was a power amplifier disjointed from a Motorola brand repeater (Micro Base and Repeater Stations 132–174 MHz, 68P81036E40-B) and was purchased from Junk Yard and Wouxun brand. A KG-UVD1P model hand-held transceiver was used as the exciter. A manual power control circuit was added to adjust power in the range of 5–200 W. The antenna employed in this study was handmade according to the given project in American Radio Relay League (ARRL). The antenna was also tested to determine minimum voltage standing wave ratios (VSWRs) by applying minimum power *via* the hand-held device. Subsequently, the antenna was connected to the power amplifier and was checked again. Prior to application, the maximum power radiation region of the antenna was detected using a relative field strength meter and a small fluorescence lamp. These experiments indicated that a small platform around the antenna at a height of 10 cm above the antenna connection base was the most effective for inducing SPIONs with RF radiation, which was detected by an infrared thermal camera (FLIR i5, USA). Configurations of the RF generator and the hyperthermia procedure are summarized in Scheme 1.

Preliminary heating experiments

Various nanoparticles at different concentrations were placed in the PTFE-type vessel (Eppendorf shape) and were then fixed directly on the antenna to determine temperature rises as a result of RF effects. VSWR was adjusted to maintain the reflected power value at a maximum of 15% of the total RF power. Samples were induced by RF exposure at 144.015 MHz and in the range of 80–180 W, and temperatures of nanoparticle solutions were recorded for 5 min intervals using an infrared thermal camera. To simulate cell culture conditions, an isolated cabin was designed to maintain the interior temperature at 37.5 °C.

Cell viability, apoptosis and necrosis tests: the effects of nanoparticle type and RF exposure

The details of this section were given in ESI† section.

Results and discussion

Characterization of nanoparticles

Nanoparticles were characterized using transmission electron microscopy (TEM, Jem Jeol 2100 F 200 kV HRTEM) and a UV-vis (Jasco V530) spectrophotometer. Average particle sizes of the nanoparticles were determined by counting at least 100 particles for each sample in TEM images *via* free ImageJ software. TEM images of the prepared nanoparticles are shown in Fig. S1† which indicated efficient synthesis of SPIONs, Au@SPIONs, AuNPs and AuNRs. All types of nanoparticles except AuNRs were spherical. Average particle sizes of SPIONs, AuNPs, AuNRs (longitudinal) and Au@SPIONs were 10, 25, 45 and 15 nm, respectively. The average SPION size was 10 nm, and accumulated shells of gold ions on SPIONs produced Au@SPIONs of 15 nm on average.

SPR properties of nanoparticles were determined using UV-vis spectrophotometry (Fig. S2†). No SPR characteristic peak was observed for SPIONs (data not shown). Synthesis of AuNPs and presence of gold shells on Au@SPIONs were confirmed by absorption peaks at wavelengths of 527 and 532 nm, respectively. Extinction peaks at 526 and 753 nm correspond to transverse and longitudinal plasmon bands of AuNRs with an aspect ratio of approximately 3, respectively. Taken together, TEM images and UV-vis data indicated that all nanoparticles were prepared efficiently and had the desired structures and sizes.

Preliminary heating experiments

Cell-free nanoparticle solutions of varying concentrations were exposed to RF at different powers and hyperthermic temperature rises were detected using a thermal camera as depicted in Fig. S3† for the case of 180 W RF and 30 μg ml^{-1} nanoparticle solutions over time. Nanoparticle-free (DI water) sample was used as control group sample (Fig. 1). This observation clearly depicted that heating in nanoparticle-containing solutions is power-dependent and sufficient to induce cell death through hyperthermia. RF-exposed nanoparticle solutions were heated following absorption of RF wave energy. The mechanism of heating was formulated according to the Joule Rule and SAR as follows:[25]

$$dT/dt = [\delta(\omega)nad|E|^2]/VC_w \quad (1)$$

$$SAR = CdT/dt \quad (2)$$

where dT/dt is the temperature gradient against time, δ is the conductivity of nanoparticles, n is the number of nanoparticles, a is the cross-section of nanoparticle, d is the nanoparticle diameter, $|E|$ is the field strength in the host dispersion, V is the volume of nanoparticles dispersion, C_w is the heat capacity of water and C is the heat capacity of the nanoparticle solution. The Joule's nanoparticles heating model is dependent on the

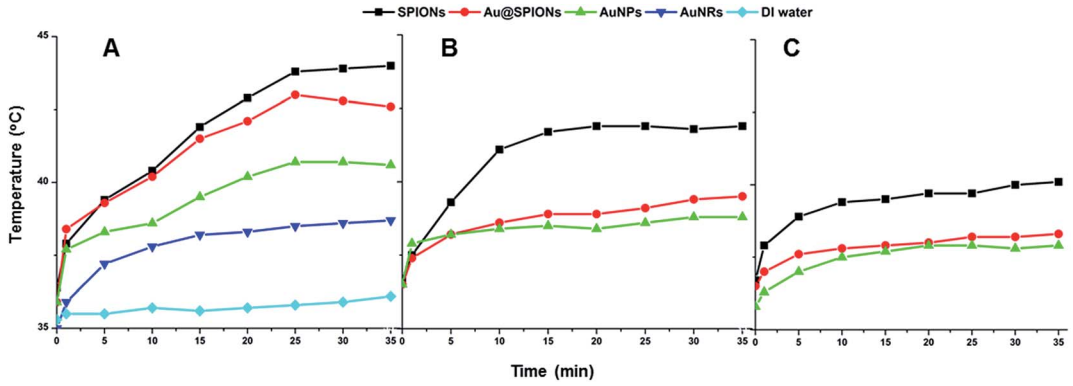

Fig. 1 Temperature rise curves in the presence of 30 μg ml^{-1} of nanoparticle concentration with (A) 180 W, (B) 120 W and (C) 80 W RF powers.

size and structure of nanoparticles so that smaller nanoparticles have higher heating efficiency than larger nanoparticles.[25] In addition, increasing RF power and nanoparticle concentration results in greater temperature rises (Fig. 1, S4, and S5†). At equal concentrations, SPIONs are present at remarkably higher numbers than other nanoparticles due to their smaller size. Moreover, according to the Joule model[25] and SAR mechanism,[26] the number density of nanoparticle material is critical to its hyperthermic action. In addition, characteristics of SPIONs, such as dielectric coefficients and conductivity factors, led to higher temperature rises compared with similar-sized nanoparticles. Accordingly, while SPIONs produced the highest temperature (43.6 °C), AuNRs led to the lowest temperature (39 °C; Fig. 1A). Because of inappreciable temperature rises of AuNRs approximately 2.5 °C, cell-based RF studies of AuNR were omitted. The poor heating efficiency of nanorods may be attributed to their bigger sizes compared to other nanoparticles. The hyperthermic efficiency of Au@SPIONs was between that of SPIONs and AuNPs, reflecting the characteristics of gold and SPIONs. Specifically, smaller temperature rises were detected because of lower nanoparticle concentrations (5 and 15 μg ml^{-1} of nanoparticle; Fig. S4 and S5†). In addition to Joule Rule and SAR mechanism, different mechanisms have been proposed to explain generation of heat for different nanoparticle types. For the case of gold nanoparticles, Moran *et al.* reported that the Joule model can be applied to gold nanoparticles.[25] The good correlation between the theoretical and experimental RF induced heating rates proved Joule heating of gold nanoparticles by capacitively coupled RF fields for smaller nanostructures. However, Liu *et al.* reported that none of the heating mechanism including dielectric loss, Joule heating or Mie theory does not support the heating of gold nanoparticles under 13.56 MHz RF field.[16] They depicted that the impurities in nanoparticle solution contribute more than gold nanoparticles under the same conditions. The heating of gold nanoparticles under RF exposure is still scientific phenomena and needs further experimental and theoretical studies to be revealed. Specifically, magnetic nanoparticles such as iron oxide nanoparticles generate heat as result of two mechanisms: Brownian relaxation (particle rotation) and Neél relaxation (magnetic moment rotation). While Brownian relaxation occurs in all nanoparticles, Neél relaxation is observed in superparamagnetic nanoparticles. Brownian relaxation is given by:

$$\tau_b = (4\pi\eta r)/(k_B T) \quad (3)$$

where T is the temperature, η is the dynamic viscosity of liquid, r is the hydrodynamic radius and k_B is Boltzmann constant. Neél relaxation is given by:

$$\tau_N = \tau_o\, e^{(\Delta E/k_B T)} = \tau_o\, e^{(KV/k_B T)} \quad (4)$$

where τ_o is in the order of 10^{-9} s and ΔE is the anisotropic energy barrier equal to the product of an effective anisotropic energy constant (K) and volume (V). These observations demonstrated that physicochemical properties, such as size, chemical structure and concentration as well as RF power are primary determinants of temperature rises in studies of nanoparticle-mediated hyperthermia.

Cell viability tests: the effects of nanoparticle type and RF exposure power

Toxic effects of SPION, Au@SPION and AuNP at various concentrations were determined in fibroblast and breast cancer cells. As shown in Fig. 2, cell viability (toxicity) in both fibroblast and breast cancer cells was highly dependent on nanoparticle concentration and type as well as RF power. Cell death index was almost insignificant at low concentrations of nanoparticles (5 μg ml^{-1}) without RF exposure (Fig. 2). However, increased nanoparticle concentrations (30 μg ml^{-1}) led to marked decreases in cell viability of both cell lines. In the absence of RF exposure, cell viability was the lowest in the presence of 30 μg ml^{-1} SPIONs and was reduced to 65.3% ± 0.7% and 69.4% ± 1.6% in fibroblast and breast cancer cells, respectively. This result indicates that despite of their reported biocompatibility, metal-based nanoparticles are toxic, particularly at high concentrations. RF exposure resulted in marked reductions in cell viability in both cell lines, and 180 W RF exposure with 30 μg ml^{-1} SPIONs decreased viability to 23.6% ± 5.2% and 43.5% ± 2.3% in breast cancer and fibroblast cells, respectively (Fig. 2). In almost all cases, increased nanoparticle concentration and RF power led to lower cell viability, confirming the biological

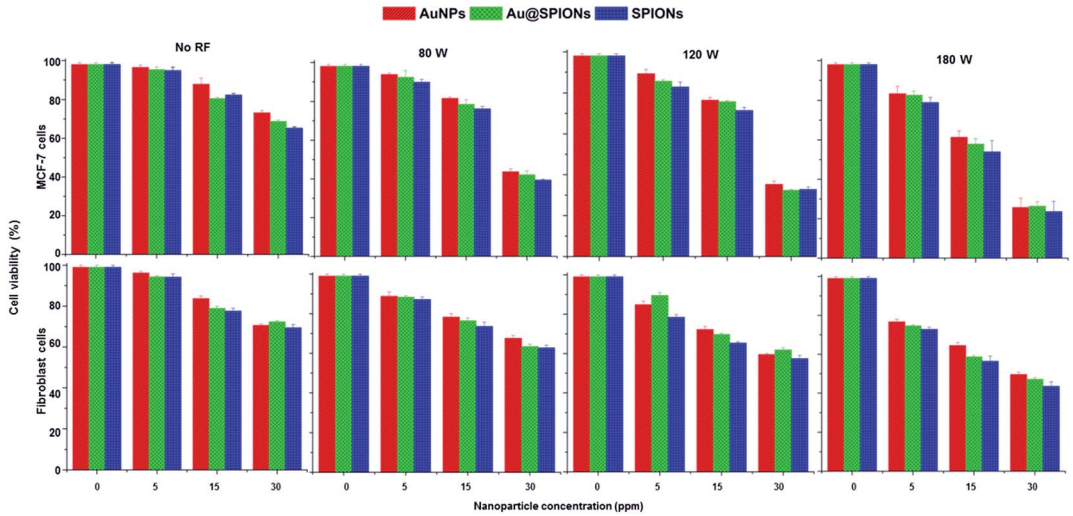

Fig. 2 Cell viability indexes of MCF-7 and L-929 cells treated with nanoparticles in the absence and presence of different RF power exposures; cell viability was assessed by using WST-1.

relevance of the present temperature rise experiments. Similarly, SPIONs produced the highest RF radiation-dependent cytotoxic effects. Additionally, much more sophisticated nature of breast cancer cells than fibroblast cells suggested greater sensitivity to hyperthermic temperature changes under the same experimental conditions.[5,6] Morphological changes in fibroblast (L-929) and cancer cells (MCF-7) in the presence of 30 μg ml^{-1} SPIONs before and after RF exposure are shown in Fig. S6.† Prior to RF exposure, fibroblast cells had regular shapes and focal adhesion. Although the toxicity of SPIONs alone was observed in minority of cells to some extent, subsequent RF exposure caused marked changes in cell morphology because of cell lysis.[27,28]

Apoptosis and necrosis tests: the effects of nanoparticle type and RF exposure

Apoptosis and necrosis of MCF-7 cells (Fig. 3) and L-929 cells (Fig. 4) were assessed after various RF powers exposures as well as nanoparticle concentrations; the results correlated well with cell viability indexes. In the absence of RF exposure as a control group, nanoparticles at lower concentrations caused little apoptosis and necrosis in either cell line. Similarly, RF exposure without nanoparticles had only slight effect on apoptosis and necrosis indexes (<10%) in all experiments. However, in the presence of nanoparticles with 80 W and 120 W RF power led to remarkable increases in apoptosis and necrosis in both cell lines. At maximal RF power (180 W; Fig. 3 and 4), the highest

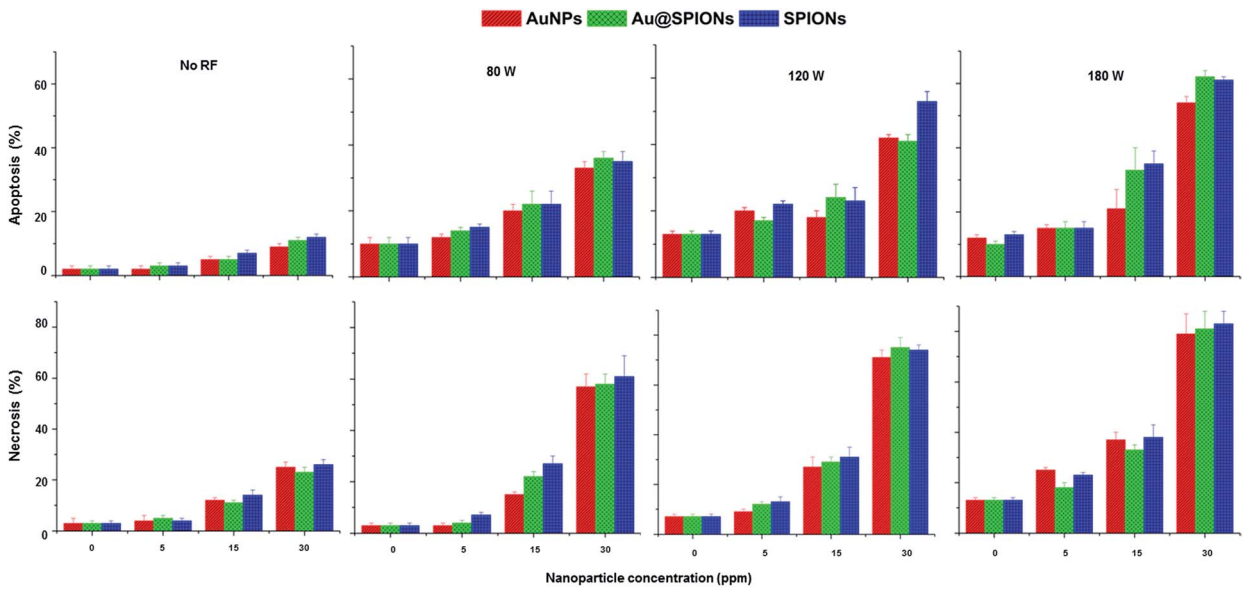

Fig. 3 Apoptosis and necrosis indexes of MCF-7 cells obtained by double staining after treatment with nanoparticles in the absence and presence of different RF power exposure.

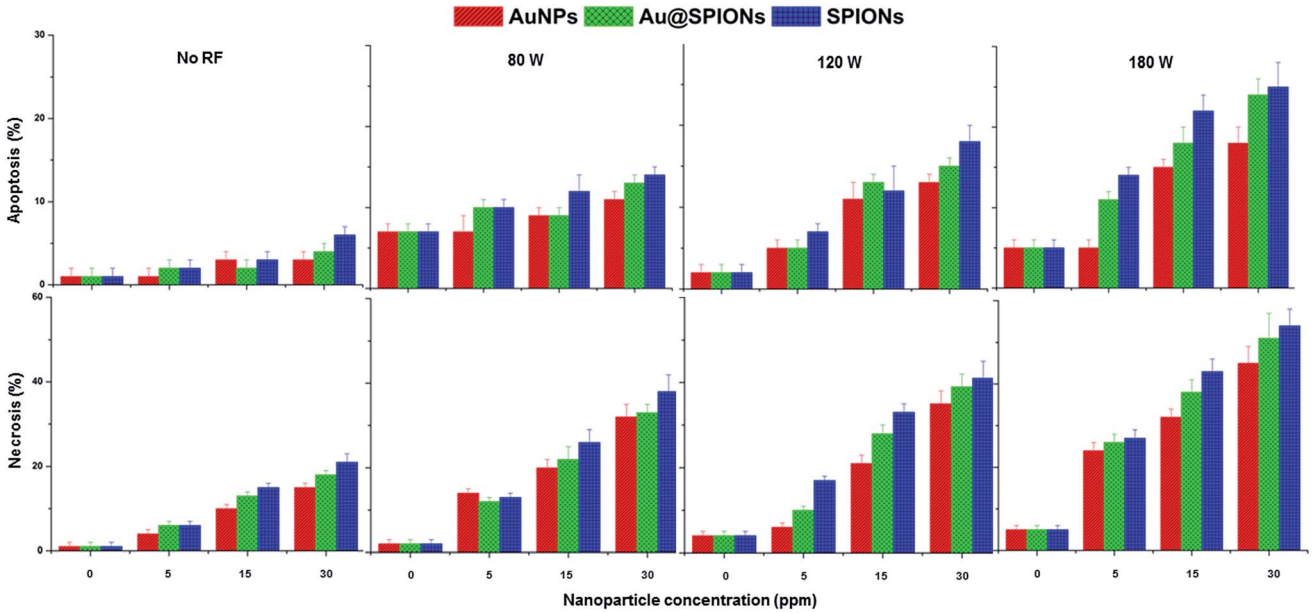

Fig. 4 Apoptosis and necrosis indexes of fibroblast cells obtained by double staining after treatment with nanoparticles in the absence and presence of different RF power exposure.

values of apoptosis and necrosis were recorded in the presence of 30 μg ml^{-1} SPIONs for MCF-7 cells 62% and 85%, respectively, and for L-929 cells 26% and 55%, respectively. The persistently higher prevalence of apoptosis over necrosis may reflect the differences in associated mechanisms. Apoptosis is defined as cell cycle arrest and induction of DNA repair machinery, whereas necrosis refers to cell damage that is beyond repair. Thus, the apoptotic programmed cell death response is highly cell-specific and is the predominant form of physiological cell death in multicellular organisms.[29] In contrast, necrosis lacks features of apoptosis and autophagy and is usually considered uncontrolled.[30] Studies of apoptosis and necrosis indicated that MCF-7 cells had higher apoptotic and necrotic indexes than fibroblast cells under identical experimental conditions as depicted in the previous observation.

Representative fluorescence images of apoptotic and necrotic MCF-7 and L929 cells before and after RF exposure are shown in Fig. 5 and 6, respectively. In images of apoptotic cells, nuclei of normal cells are stained with low-intensity blue fluorescence, while apoptotic cells stained with Hoechst 33342 dye show stronger fluorescence. Apoptotic cells were also identified according to morphological changes in the nucleus, which indicate nuclear fragmentation and chromatin condensation. Exposure to RF resulted in remarkable changes in the morphology and nuclei of MCF-7 and L-929 cells and apoptosis was explicitly detected (Fig. 5). Similar changes were observed in the studies of necrosis (Fig. 6), where marked increases were observed in the numbers of necrotic cells after exposure to RF in both cell lines.

Considering all *in vitro* tests, we strongly anticipate that the application of antenna-type RF generator in clinical applications would offer remarkable advantages compared to available counterparts (*i.e.* inductive modulus and capacitive coupled RF generators). Firstly, the proposed home-made RF generator is user friendly, reliable, simple, and low-cost. In clinical uses, the patient would sit in an isolated cabin surrounded with RF antennas during RF exposure. The number of antennas, distance to patient as well as power of RF generator can be manipulated without discomfort of the patient which is

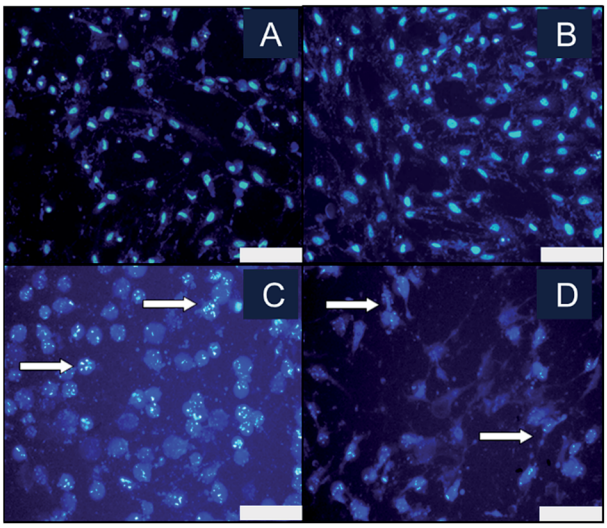

Fig. 5 Apoptosis fluorescence microscopy images of MCF-7 and L-929 cells. MCF-7 (A, 12% apoptosis) and L-929 cells (B, 6% apoptosis) treated with 30 μg ml^{-1} SPIONs without RF exposure; MCF-7 (C, 62% apoptosis) and L-929 cells (D, 26% apoptosis) treated with 30 μg ml^{-1} SPIONs and 180 W RF. Fluorescence microscopy images were taken at 100× magnification using a Leica DMI6000 model inverted microscope. Bars indicate 200 μm. Arrows indicate apoptotic changes in the cells.

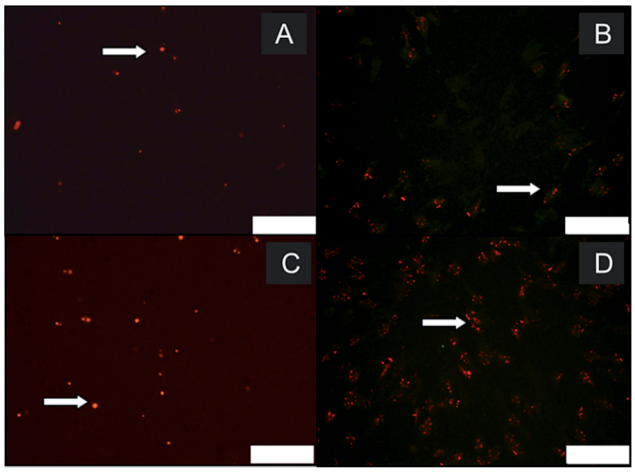

Fig. 6 Necrosis fluorescence microscopy images of MCF-7 and L-929 cells. MCF-7 (A, 26% necrosis) and L-929 cells (B, 21% necrosis) treated with 30 μg ml^{-1} SPIONs without RF exposure; MCF-7 (C, 85% necrosis) and L-929 cells (D, 54% necrosis) treated with 30 μg ml^{-1} SPIONs and 180 W RF. Necrotic cells can be identified by red PI-stained nuclei, as indicated by arrows; fluorescence microscopy images were taken at 100× magnification using a Leica DMI6000 model inverted microscope. Bars indicate 200 μm.

inevitable for other type RF generators. The flexibility of the proposed system would prevent the undesired effects on patients such as claustrophobia. Also, we did not observe any temperature increase along the antenna which prevents the application of device during RF exposure in other type RF generators. In inductive type RF generators, back reflected RF waves cause heat generation on bobbin and dramatically decreases RF power. For the case of nanoparticle-mediated hyperthermia, the nanoparticles can be injected to vein *via* active targeting or direct injection to tumor *via* passive targeting. In the following studies, the effects of basic parameters of on *in vivo* studies will be determined by employing proper methods. It is quite reasonable to expect the adequate performance of antenna-type RF generator considering non-ionized, non-destructive, and non-harmful energy band of electromagnetic spectrum with appropriate penetration depths into the body for the deep hyperthermia of the seated tumors. Although the proposed RF generator system provides impressive advantages, there are some issues to be concerned before its clinical applications. The lack of focus control of the RF triggered waves in the interest region (cancerous tissue) and the synthesis of nanoparticles with desired size and morphology are critical problems that should be eliminated.

Conclusion

This study demonstrates that non-invasive RF hyperthermia employing an antenna-type RF generator using different types of nanoparticles such as SPIONs, Au@SPIONs, AuNPs and AuNRs with various properties and structures is a potentially novel cancer treatment method. Our preliminary heating studies demonstrated adequate temperature rises for all RF-exposed nanoparticles except AuNRs. *In vitro* assays indicated that colloidal nanoparticles are not directly cytotoxic especially at low concentrations. However, at high concentrations, cell viability was remarkably decreased by nanoparticles concentration upon RF exposure. The temperature rise and viability, apoptosis and necrosis of cells can be manipulated by changing RF power and concentration of nanoparticle solution over time. The present study paved the way for further investigations that cover modified nanoparticles to be used in targeted hyperthermia for *in vivo* applications using the present antenna-type RF generator. The different characteristics of nanoparticles (magnetite and gold) serve significant flexibility to bioconjugation of nanoparticles with antibody or aptamer molecules to bind to cancer cells particularly. In conclusion, this study proved that a reliable, simple, low-cost and home-made antenna-type RF generator combined with basic nanoparticles in different structures and characteristics is a powerful candidate for hyperthermia studies and would be a competitive alternative to sophisticated and expensive counterparts such as inductive and capacitive RF generators.

Acknowledgements

EP also acknowledges support from the Turkish Academy of Science as a full member. The authors also wish to thank the Department of Molecular Biology and Genetics (Bilkent University, Turkey) and the Sap Institute (Ankara, Turkey) for supplying the cell lines.

Notes and references

1 S. A. Rosenberg, *Cancer Res.*, 1991, **51**, 5074s–5079s.
2 P. Cherukuri, E. S. Glazer and S. A. Curley, *Adv. Drug Delivery Rev.*, 2010, **62**, 339–345.
3 L. Zhao, J. Tang and S.-S. Feng, *Nanomedicine*, 2010, **5**, 1305–1308.
4 C. D. Kaddi, J. H. Phan and M. D. Wang, *Nanomedicine*, 2013, **8**, 1323–1333.
5 J.-L. Li and M. Gu, *IEEE J. Sel. Top. Quantum Electron.*, 2010, **16**, 989–996.
6 J. van der Zee, *Ann. Oncol.*, 2002, **13**, 1173–1184.
7 L. Asin, M. Ibarra, A. Tres and G. Goya, *Pharm. Res.*, 2012, **29**, 1319–1327.
8 M. Falk and R. Issels, *Int. J. Hyperthermia*, 2001, **17**, 1–18.
9 P. C. Chen, S. C. Mwakwari and A. K. Oyelere, *Nanotechnol., Sci. Appl.*, 2008, **1**, 45.
10 E. Boisselier and D. Astruc, *Chem. Soc. Rev.*, 2009, **38**, 1759–1782.
11 T. L. Doane and C. Burda, *Chem. Soc. Rev.*, 2012, **41**, 2885–2911.
12 N. Tran and T. J. Webster, *J. Mater. Chem.*, 2010, **20**, 8760–8767.
13 R. Sharma and C. Chen, *J. Nanopart. Res.*, 2009, **11**, 671–689.
14 C. S. Kumar and F. Mohammad, *Adv. Drug Delivery Rev.*, 2011, **63**, 789–808.
15 M. A. El-Sayed, *Acc. Chem. Res.*, 2001, **34**, 257–264.

16 X. Liu, H.-j. Chen, X. Chen, C. Parini and D. Wen, *Nanoscale*, 2012, **4**, 3945–3953.
17 S. Cho, K. Emoto, L.-J. Su, X. Yang, T. Flaig and W. Park, *J. Biomed. Nanotechnol.*, 2014, **10**, 1267–1276.
18 C. J. Trujillo-Romero, S. Garcia-Jimeno, A. Vera, L. Leija and J. Estelrich, *Prog. Electromagn. Res.*, 2011, **121**, 343–363.
19 D. E. Kruse, D. N. Stephens, H. A. Lindfors, E. S. Ingham, E. E. Paoli and K. W. Ferrara, *IEEE Trans. Biomed. Eng.*, 2011, **58**, 2002–2012.
20 C. J. Gannon, C. R. Patra, R. Bhattacharya, P. Mukherjee and S. A. Curley, *J. Nanobiotechnol.*, 2008, **6**, 2.
21 J. Cardinal, J. R. Klune, E. Chory, G. Jeyabalan, J. S. Kanzius, M. Nalesnik and D. A. Geller, *Surgery*, 2008, **144**, 125–132.
22 E. S. Glazer, C. Zhu, K. L. Massey, C. S. Thompson, W. D. Kaluarachchi, A. N. Hamir and S. A. Curley, *Clin. Cancer Res.*, 2010, **16**, 5712–5721.
23 M. Raoof, S. J. Corr, W. D. Kaluarachchi, K. L. Massey, K. Briggs, C. Zhu, M. A. Cheney, L. J. Wilson and S. A. Curley, *Nanomedicine*, 2012, **8**, 1096–1105.
24 T. Mustafa, Y. Zhang, F. Watanabe, A. Karmakar, M. P. Asar, R. Little, M. K. Hudson, Y. Xu and A. S. Biris, *Biomater. Sci.*, 2013, **1**, 870–880.
25 C. H. Moran, S. M. Wainerdi, T. K. Cherukuri, C. Kittrell, B. J. Wiley, N. W. Nicholas, S. A. Curley, J. S. Kanzius and P. Cherukuri, *Nano Res.*, 2009, **2**, 400–405.
26 G. Hanson, R. Monreal and S. P. Apell, *J. Appl. Phys.*, 2011, **109**, 124306.
27 P. J. Mohr, B. N. Taylor and D. B. Newell, *J. Phys. Chem. Ref. Data*, 2012, **41**, 043109.
28 R. Ghosh, L. Pradhan, Y. P. Devi, S. Meena, R. Tewari, A. Kumar, S. Sharma, N. Gajbhiye, R. Vatsa and B. N. Pandey, *J. Mater. Chem.*, 2011, **21**, 13388–13398.
29 R. P. Rastogi, Richa and R. P. Sinha, *EXCLI Journal*, 2009, **8**, 155–181.
30 P. Golstein and G. Kroemer, *Trends Biochem. Sci.*, 2007, **32**, 37–43.

